

# Energy Transfer versus Charge Separation in Type-II Hybrid Organic–Inorganic Nanocomposites

Andrey A. Lutich, Guoxin Jiang, Andrei S. Susha, Andrey L. Rogach, Fernando D. Stefani,\* and Jochen Feldmann

Photonics and Optoelectronics Group, Physics Department and Center for Nanoscience (CeNS), Ludwig-Maximilians-Universität München, Amalienstrasse 54, D-80799 Munich, Germany

Received March 27, 2009; Revised Manuscript Received June 1, 2009

## ABSTRACT

Hybrid organic–inorganic nanomaterials have the potential of providing synergetic properties. Blends of semiconductor nanocrystals and conjugated polymers in particular promise novel optoelectronic properties. Effective design of tailored optoelectronic properties requires a deep understanding of the photophysics of these composite materials, which includes charge separation and Dexter and Förster energy transfer. We performed a detailed and quantitative spectroscopic investigation of a type II aligned hybrid system consisting of a blue emitting conducting polymer and CdTe nanocrystals. Although charge separation is expected from the type II alignment, we find a dominant (70% efficiency) energy transfer process. We discuss all possible de-excitation pathways for the excitons in terms of the alignment of energy levels, time scales, and physical geometry of the system. This allows us to conclude that energy transfer occurs via the Förster mechanism and provides a clear guideline for the design of novel hybrid materials.

Hybrid organic–inorganic nanomaterials have recently attracted great attention due to the appealing possibility of synergetic properties exploiting the best of both components. In particular, blends of semiconductor nanocrystals (NCs) and conjugated polymers stand out as candidates to obtain materials tailored for applications in, for example, light-emitting devices<sup>1–4</sup> and photovoltaics.<sup>5–8</sup> In comparison to organic emitters, semiconductor NCs have a number of advantages such as high photostability, broad spectral range of light absorption, and narrow emission line width.<sup>9,10</sup> The conduction properties of closely packed NC films are on the other hand poor,<sup>11</sup> making inefficient the electrical pumping of NCs. An evident approach to overcome this difficulty is to produce a composite material where the NCs provide their efficient luminescence and a conducting polymer provides efficient charge conduction.<sup>12,13</sup> From a technological viewpoint, such a polymer-based nanocomposite material offers the potential for efficient electrical pumping and relative ease of chemical processing,<sup>14</sup> which is compatible with the colloidal chemistry of NCs. However, the effective design of tailored optoelectronic properties remains challenging because the photophysics of these organic–inorganic hybrid materials, which include charge separation and Dexter and Förster energy transfer (ET),<sup>15</sup> remains to be fully understood.

In particular, an apparent controversy has been raised recently since different reports identify a dominant Förster<sup>16–18</sup> or Dexter<sup>19</sup> mechanism for the ET from conjugated polymers to semiconductor NCs in solid films. The solid samples often make difficult the separation of the effects caused by polymer-NC interaction from the other effects associated to, for example, aggregation of NCs or stacking of polymer molecules. Moreover, although it is crucial for the photo-physical understanding of these systems, the role of the alignment of the highest occupied molecular orbital (HOMO) and lowest unoccupied molecular orbital (LUMO) levels of the organic and inorganic components has not been properly addressed yet.

Here, we report on a detailed investigation of the photophysics of a hybrid organic–inorganic semiconductor system in solution. The hybrid nanocomposite consists of short (10–20 r.u.) molecules of water-soluble, conducting copolymer poly[9,9-bis(3'-((*N,N*-dimethyl)-*N*-ethylammonium)-propyl)-2,7-fluorene-alt-1,4-phenylene] dibromide (PDFD, Figure 1a) and thioglycolic acid capped, 2.7 nm CdTe NCs (Figure 1b). Steady-state and time-resolved photoluminescence (PL) measurements supported by modeling of the recombination kinetics allows us to quantitatively determine the efficiencies of the energy transfer and charge separation processes in the hybrid organic–inorganic nanocomposite. The photophysical behavior of the hybrid system is discussed

\* To whom correspondence should be addressed. E-mail: fernando.stefani@physik.uni-muenchen.de.

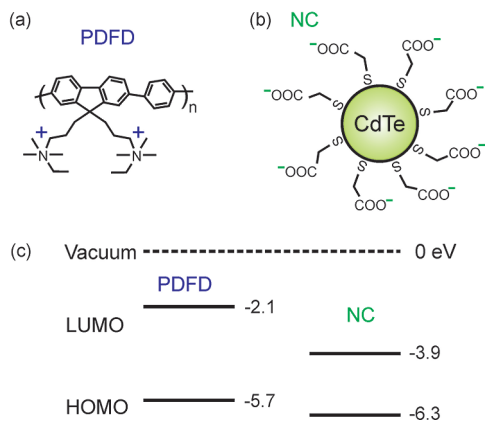


**Figure 1.** Components of the organic–inorganic semiconductor hybrid nanocomposite. (a) Repeat unit of the poly[9,9-bis(3'-(*N,N*-dimethyl)-*N*-ethylammonium)-propyl)-2,7-fluorene-alt-1,4-phenylene] dibromide (PDFD). (b) Schematic representation of a CdTe NC capped with thioglycolic acid. (c) Experimentally determined positions of the HOMO–LUMO levels (eV) of PDFD and the CdTe NCs.

in terms of the HOMO–LUMO alignment as well as the spatial configuration of the hybrid system, providing guidelines for the efficient design of its optoelectronic properties.

PDFD molecules were conjugated to the CdTe NCs by electrostatic interaction of the negatively charged surface ligands of the NCs and the positively charged side-chains of the PDFD (Figure 1a,b). The NCs and PDFD were mixed in water in equal molar concentrations ( $2 \times 10^{-7}$  M), leading to an average of one PDFD molecule bound to one CdTe NC. The absolute positions of the LUMO and HOMO levels of the PDFD are known.<sup>20</sup> The HOMO level of the CdTe NCs was determined by cyclic voltammetry and the position of the LUMO level was obtained by adding to the HOMO position the band gap determined by optical absorption measurements. The type II alignment of the HOMO and LUMO levels of NCs and PDFD makes evident the possibility of charge separation (Figure 1c). The offset of the LUMO levels is much larger than the HOMO levels difference, which should favor electron transfer from PDFD to NC with respect to hole transfer from NC to PDFD.

In addition to the possibility of charge separation, the total spectral overlap of the blue emission of PDFD and the absorption of CdTe NCs provides favorable conditions for ET from the PDFD to NCs, which is confirmed by the steady-state spectra shown in Figure 2. The absorption of equal concentration solutions of bare NCs, bare PDFD, and of the PDFD-NC composite are shown in Figure 2a. For wavelengths above 450 nm, where the PDFD absorption is negligible, the absorption spectrum of the PDFD-NC composite coincides with the spectrum of bare NCs, indicating that the intrinsic electronic structure of the NCs is not affected by conjugation to the PDFD. This is further supported by the PL excitation (PLE) measurements (Figure 2b) recorded at the peak emission wavelength of the NCs of 545 nm. For excitation wavelengths longer than ca. 450 nm only the NCs in the PDFD-NC composite are excited and behave identically to bare NCs. As the excitation wavelength is reduced beyond 450 nm, the PDFD molecules begin to

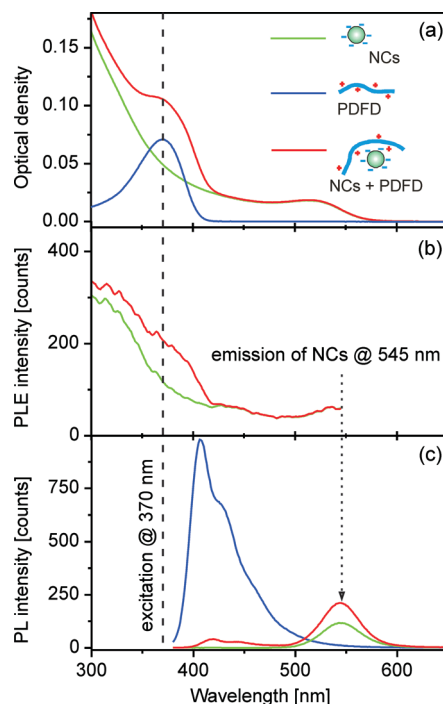


**Figure 2.** Steady-state spectra of bare CdTe NCs (green), bare PDFD (blue) and the PDFD-NC composite (red). (a) Absorption. (b) PLE at the emission wavelength of 545 nm. (c) PL at the excitation wavelength of 370 nm.

absorb light and transfer energy to the NCs, which results in a higher PLE signal. The ET transfer process is also evident in the PL spectra at an excitation wavelength of 370 nm (Figure 2c). Upon conjugation to the NCs, the PL of the PDFD is strongly quenched (24-fold) and the PL intensity of the NCs is almost doubled. At an excitation wavelength of 470 nm, where PDFD does not absorb, the PL spectrum of the composite and of bare NCs are identical (not shown), which proves that not only the intrinsic absorption but also the PL properties of the NCs remain intact in the hybrid system. The emission of PDFD in the PDFD-NC system presents a 95 meV red shift with respect to the emission of bare PDFD. Similarly, subtraction of the NC absorption from the absorption of the PDFD-NC system shows the absorption of PDFD in the complex is red-shifted too, in this case by 60 meV. This effect could be attributed to the local charges of the NC surface or conformational changes of the polymer upon binding to the NC. Since these red-shifts are small in comparison to the energy of the HOMO and LUMO levels, they can be neglected in band alignment considerations. Nevertheless, they must be taken into account in accurate ET calculations.

Phenomenologically, the ET efficiency is calculated as the number of acceptors (NCs) excited via ET divided by the number of excited donors (PDFD molecules). Thus, ET efficiency may be estimated both from the reduction of the PDFD PL or the increase in NC PL. If ET is the only process additional to the spontaneous decay that depopulates the excited state of PDFD, the two ET efficiency calculations should give the same result. Considering the NC PL increase, the ET efficiency may be calculated using the following relation:<sup>21</sup>

$$\Phi_{\text{ET}} = \frac{A_{\text{NC}}(\lambda_{\text{exc}})}{A_{\text{PDFD-NC}}(\lambda_{\text{exc}}) - A_{\text{NC}}(\lambda_{\text{exc}})} \left( \frac{I_{\text{NC}}}{I_{\text{NC}}^0} - 1 \right) \quad (1)$$

where  $A_{\text{NC}}(\lambda_{\text{exc}})$  and  $A_{\text{PDFD-NC}}(\lambda_{\text{exc}})$  are the absorption of the bare NCs and of the PDFD-NC composite, respectively, at the wavelength of excitation  $\lambda_{\text{exc}}$ .  $I_{\text{NC}}^0$  and  $I_{\text{NC}}$  are the integrated PL intensities of the NCs in absence and presence of the PDFD, respectively. Applying the formula 1 to the PL spectra of NCs,  $\Phi_{\text{ET}}$  equals 72%.

Alternatively, ET efficiency may be calculated from the PDFD PL quenching by

$$\Phi_{\text{ET}} = 1 - \frac{A_{\text{PDFD}}(\lambda_{\text{exc}})}{A_{\text{PDFD-NC}}(\lambda_{\text{exc}}) - A_{\text{NC}}(\lambda_{\text{exc}})} \cdot \frac{I_{\text{PDFD}}}{I_{\text{PDFD}}^0} \quad (2)$$

where  $A_{\text{PDFD}}(\lambda_{\text{exc}})$  is absorption of bare PDFD at the wavelength of excitation  $\lambda_{\text{exc}}$ .  $I_{\text{PDFD}}^0$  and  $I_{\text{PDFD}}$  are the integrated PL emission of PDFD when excited at  $\lambda_{\text{exc}}$  in absence and presence of NCs, respectively. The term  $A_{\text{PDFD-NC}}(\lambda_{\text{exc}}) - A_{\text{NC}}(\lambda_{\text{exc}})$  represents the absorption of PDFD in the PDFD-NC system. Applying the formula 2 to the PL spectra of PDFD,  $\Phi_{\text{ET}}$  equals 94%.

The estimate of the ET efficiency of 72% based on the NCs' PL increase characterizes the number of additional excitons created in the NCs due to the interaction with the PDFD. On the other hand, the more efficient, 94% PL quenching of PDFD is indicative of additional process/es taking place in the depopulation of the excited PDFD.

Further insights into the relaxation kinetics of the system are obtained by time-resolved PL measurements. In Figure 3, the PL decays of PDFD after pulsed excitation are shown for the bare PDFD and for the PDFD-NC composite. The decay of PDFD (blue) is monoexponential with a rate of  $1/470 \text{ ps}^{-1}$  (black solid line). The emission of PDFD in the PDFD-NC composite (orange) is significantly faster and indicates the presence two subensembles in the PDFD-NC blend. A fraction of 78% of the PDFD molecules decays rapidly with a rate of  $1/48 \text{ ps}^{-1}$  and the remaining 22% decays with a slower rate of  $1/210 \text{ ps}^{-1}$ .

Next, in order to understand the role of the two subensembles on the photophysical behavior of the hybrid system, we investigate the time-resolved PL of the NCs on the same time scale where the PDFD decays (Figure 4). Time-resolved PL kinetics of bare NCs solution (green squares) and of NCs in the PDFD-NC composite solution (red circles) were integrated in the spectral window from 540 to 560 nm at excitation wavelength of 370 nm. The PL decay of bare CdTe NCs in water is multiexponential,<sup>22</sup> a common feature of semiconductor NCs whose mechanism is still under debate.<sup>23,24</sup> The intrinsic exciton dynamics of CdTe NCs is not in the focus of this article so we adequately model the relaxation dynamics of the CdTe NCs with a double-exponential that is then used as a reference for comparison to the dynamics of the NCs in PDFD-NC composite. The solid line in the Figure 4 represents simulated PL kinetic of bare NCs having two decay rates:  $1/11 \text{ ns}^{-1}$  and  $1/75 \text{ ps}^{-1}$ . The PL kinetics of the NCs in the PDFD-NC composite

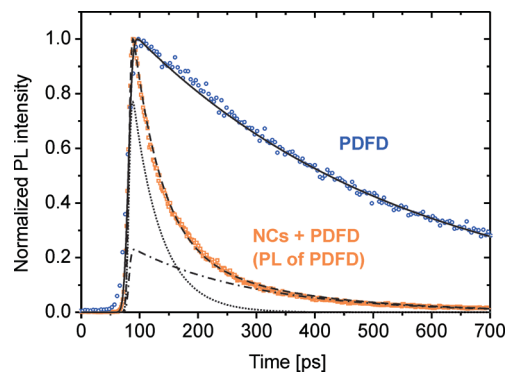


**Figure 3.** Time-resolved PL of bare PDFD (blue) and of PDFD in the PDFD-NC composite (orange). The PL was excited at 370 nm and integrated in the spectral window from 390 to 440 nm. The black curves are the modeled PL evolution including the excitation pulse and the system response. The decay of bare PDFD can be modeled with a single decay constant of 470 ps. Modeling of the PDFD decay in the composite requires two decay constants of 48 ps (78%) and 210 ps (22%).

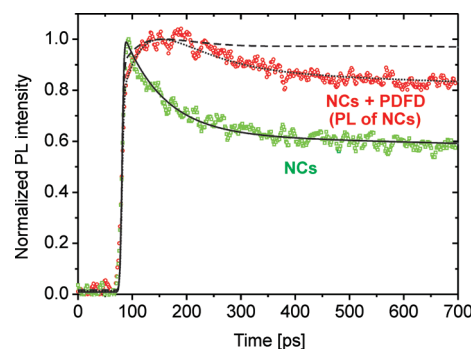


**Figure 4.** Time-resolved PL of bare CdTe NCs (green) and of the NCs in the PDFD-NC composite (red). The PL was excited at 370 nm and integrated in the spectral window from 540 to 560 nm. The black curves are the modeled PL evolution including the excitation pulse and system response. The solid line is a double exponential modeling of the bare NC decay which is used as a reference for the modeling of the NC decay in the PDFD-NC composite (long- and short-dashed curves).

under the same conditions exhibits a much slower build-up, which is a result of the additional excitation of the NCs by means of the ET from PDFD molecules to NCs. In order to quantify the ET, we modeled the time dependent PL of the NCs in PDFD-NC composite using the decay parameters of bare NCs and introducing an additional excitation channel corresponding to the ET. In the low pump intensity regime of our experiments, the probability of the ET from the PDFD to the NCs is proportional to the excited state population of PDFD. The time-dependent excited state population of PDFD is known from the time-resolved PL measurements. Therefore, we introduce in our rate equations model an additional excitation of the NCs with the temporal profile of the PL decay of PDFD in the PDFD-NC composite with a certain coefficient. This coefficient is not a free parameter but should be consistent with the relative PL increase of NCs due to the ET with respect to direct excitation of NCs observed in steady-state experiments. This condition is satisfied when the ratio between the integral of the temporal profile of the direct excitation and the integral of the temporal profile of

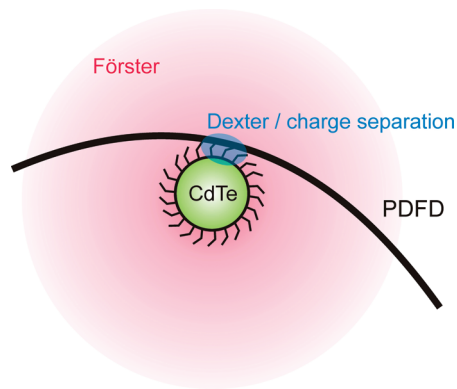


**Figure 5.** Schematic of the geometry of the PDFD-NC system and of the regions for Förster energy transfer (red) and for charge separation or Dexter energy transfer (blue).

the ET is 1/0.8. At this point, we recall that in the PDFD-NC composite, two subensembles of PDFD molecules are present. Therefore, we performed simulations of PL kinetics of the NCs in the PDFD-NC composite using as temporal ET profile (i) the total PDFD kinetic (Figure 3 dashed line), that means including all PDFD molecules, and (ii) only the faster subensemble (Figure 3 short-dash line). As it can be seen in Figure 4, the simulation considering ET from all PDFD molecules (dashed line) deviates significantly from the experimental result (red circles) whereas the simulation using only faster subensemble of PDFD (short-dash line) is in excellent agreement with the measured data. We thus conclude that in the PDFD-NC system, 78% of the PDFD molecules decay via ET to the NCs with fast rate of  $1/48 \text{ ps}^{-1}$ . In the minor 22% subensemble PDFD-NC, the emission of PDFD is quenched but does not lead to PL of NCs. Although the presence of dark NCs<sup>25</sup> that may quench the emission of PDFD without emitting cannot be completely excluded, the most probable process taking place in the minor subensemble is charge separation. Charge separation is possible due to the type-II alignment of the system but unfavored by the relative large distance (minimum 1.5 nm) between the PDFD molecules and the NCs core. This minimum distance is determined by the nanocrystal size and by the length of its surface ligand molecules. Still, due to the statistical alignment of PDFD and NCs, some of the composites will have relative orientations of their excitons that make ET impossible<sup>21</sup> and in this case, a slow charge separation process may take place. A reduction of this minimum distance, for example, by removing the surface ligands, or an increase in the offsets of the energy levels may lead to a more efficient charge separation.<sup>15</sup>

The presence of the two subensembles explains the discrepancy between estimates of the ET efficiency obtained from the increase in the PL of NCs and from the decrease in the PL of PDFD. Having identified that only the major,

fastest subensemble PDFD-NC hybrids exhibit ET, the ET efficiency can be calculated as  $\Phi_{\text{ET}} = (1 - \tau_{\text{PDFD-NC}}/\tau_{\text{PDFD}}) \cdot \eta_{\text{ET}} = 70\%$ , where  $\tau_{\text{PDFD}} = 470 \text{ ps}$  is the bare PDFD lifetime,  $\tau_{\text{PDFD-NC}} = 48 \text{ ps}$  is the lifetime and  $\eta_{\text{ET}} = 78\%$  is the fraction of PDFD-NC composites presenting ET. The obtained value of 70% is in an excellent agreement with the ET efficiency of 72% calculated from NCs PL increase in steady-state experiments.

At this point we move into the discussion of the mechanism of ET from the PDFD molecules to the CdTe NCs. Previous data on ET from polymers to NCs in solid films have been discussed both within the dipole–dipole Förster energy transfer<sup>16–18</sup> and the electron exchange Dexter mechanism.<sup>19</sup> Indeed both mechanisms can act simultaneously, but it is possible to identify the dominant one based on kinetic, energetic, and spatial arguments. First, Dexter ET mechanism requires type-I alignment of HOMO and LUMO levels of the donor–acceptor pair in order to allow the simultaneous injection of electron and hole to the donor, whereas our system has a type II alignment (Figure 1c). In addition, the typical time scale of efficient Dexter ET lies in the subpicosecond range,<sup>26</sup> while we observe a much slower rate of  $1/\tau_{\text{ET}} = 1/\tau_{\text{PDFD-NC}} - 1/\tau_{\text{PDFD}}$  of  $1/53 \text{ ps}^{-1}$ . Although unusually slow Dexter ET from conducting polymers may be argued by exciton diffusion along the polymer chain to the acceptor site,<sup>19</sup> this does not apply to the short 10–20 r.u. PDFD molecules used in these experiments. Finally, likewise charge separation, Dexter ET is a short-range process and occurs efficiently at sub nanometer donor–acceptor distances because a sufficient overlap of donor and acceptor electron orbitals is required.<sup>27</sup> In the composite system studied here, based on the NC size (including surface ligands) we estimate a minimum distance between the NC core and the polymer chain of 1.5 nm. Furthermore, the Kuhn length of polymers like PDFD lies between 14 and 17 nm<sup>28,29</sup> which corresponds to the full length of the short PDFD molecules used. Thus, the PDFD is expected to behave like an elastic rod and the interaction region for Dexter ET is confined to the immediate vicinity of the NC. Förster ET on the other hand may occur over much longer distances. On the basis of the full spectral overlap of PDFD emission and NC absorption and considering an average over all possible dipole orientations of PDFD and NCs, a Förster radius of roughly 6 nm is predicted. The geometry and the regions of efficient Förster and Dexter ET in the NC-PDFD hybrid system are schematically depicted to scale in Figure 5. The efficiency of Förster energy transfer strongly depends on the relative orientation of excitons. Then, the most plausible reason why the ET efficiency does not reach 100% is the statistical relative orientation of excitons in the conducting polymer and the NCs. This in turn makes viable the occurrence of the less effective processes of charge separation.

**Table 1.** Processes Taking Place in PDFD-NC Composites with Their Corresponding Rates

process	PL decay of bare polymer	PL decay of bare CdTe NCs		PL decay of PDFD in PDFD-NC composite		energy transfer
process rate, $\text{ps}^{-1}$	1/470	1/11000	1/75	1/48	1/210	1/53
weighting factor	1	0.63	0.37	0.78	0.22	1

In conclusion, we demonstrate that in hybrid nanocomposites of semiconductor polymers and nanocrystals, with type-II alignment of HOMO and LUMO levels, the competition between energy transfer and charge separation strongly depends on the nanometric geometry of the system. The intrinsic finite size and the surface ligands of the nanocrystals impose a minimum distance between the nanocrystal core and the polymer molecules. This minimum separation limits the efficiency of charge separation and favors the occurrence of the longer range Förster energy transfer. In our system, with a minimum polymer-nanocrystal distance of 1.5 nm and a Förster radius of 6 nm, we determine a Förster energy transfer efficiency and rate of 70% and  $1/53 \text{ ps}^{-1}$ , respectively. Our experiments in solutions clearly show that tailoring the optoelectronic properties of a hybrid nanocrystal-conducting polymer nanocomposite requires a high degree of control not only on the alignment of energy levels but also on the nanoscale geometric arrangement of the components. In solid state systems, additional effects associated to, for example, aggregation of nanocrystals or stacking of polymer molecules may need to be considered.

**Materials and Methods.** CdTe NCs capped with thioglycolic acid molecules were synthesized in water as previously reported.<sup>30</sup> The water-soluble conjugated polymer (poly[9,9-bis(3'-((*N,N*-dimethyl)-*N*-ethylammonium)-propyl)-2,7-fluorene-alt-1,4-phenylene] dibromide) illustrated in Figure 1a was synthesized by following a known procedure<sup>20</sup> with a little modification. The bromo-monomer, 2,7-dibromo-9,9-bis(3'-(*N,N*-dimethylamino)propyl)fluorene, was purified by silica gel chromatography instead of recrystallization. The quaternization of the neutral precursor of the polymer was carried out in a mixture of THF and DMSO (*v/v* = 3:1). The solution was stirred at 50 °C for 5 days. During the reaction period, intermittent addition of a certain amount of water was needed to dissolve any precipitation seen in the solution in order to achieve a high yield of quaternization. After the reaction was finished, THF, water and extra bromoethane were evaporated in vacuum. The remaining DMSO solution containing the target polymer was precipitated by pouring into a large amount of ether. The precipitate was collected by centrifugation, washed with acetone, and dried overnight at 80 °C in a vacuum oven. The as-synthesized polymer inherited the advantages of excellent chemical stability and high fluorescence of classic oil-soluble polyfluorene.<sup>31</sup>

Absorption spectra were recorded using Cary 5000 UV–vis–NIR spectrometer. PL spectra were measured by Cary Eclipse fluorescence spectrometer. PL time-resolved measurements were done with a streak camera (Hamamatsu C5680) combined with the spectrometer (Cromex with 40 gr/mm grating). The Hamamatsu Syncroscan Sweep Unit M5675 and Slow Speed Sweep Unit M5677 were used to detect PL kinetics in different temporal window, from 0.5 to 100 ns, respectively. The frequency doubled output of the mode-locked titanium-sapphire laser (120 fs, 76.5 MHz) was used as an excitation source in the range from 370 to 470 nm.

The modeling of the PL kinetics was done by solving standard coupled rate equations with symbolic language Wolfram Mathematica 6.0. All simulations were done in the

low-pump regime and the population of the excited state never exceeded 0.1% of the population of the ground state.

**Acknowledgment.** We thank S. Poznyak for his valuable assistance in cyclic voltammetry measurements on CdTe NCs and acknowledge financial support of the DFG via the project RO2345/5-1, the “Nanosystems Initiative Munich (NIM)” and the “LMU<sup>excellent</sup>” program. A.A.L. and G.J. thank Alexander von Humboldt foundation for financial support.

## References

- (1) Colvin, V. L.; Schlamp, M. C.; Alivisatos, A. P. *Nature* **1994**, *370* (6488), 354–357.
- (2) Dabbousi, B. O.; Bawendi, M. G.; Onitsuka, O.; Rubner, M. F. *Appl. Phys. Lett.* **1995**, *66* (11), 1316–1318.
- (3) Tessler, N.; Medvedev, V.; Kazes, M.; Kan, S. H.; Banin, U. *Science* **2002**, *295* (5559), 1506–1508.
- (4) Koktysh, D. S.; Gaponik, N.; Reufer, M.; Crewett, J.; Scherf, U.; Eychmuller, A.; Lupton, J. M.; Rogach, A. L.; Feldmann, J. *ChemPhysChem* **2004**, *5* (9), 1435–1438.
- (5) Huynh, W. U.; Dittmer, J. J.; Alivisatos, A. P. *Science* **2002**, *295* (5564), 2425–2427.
- (6) Campbell, I. H.; Crone, B. K. *Adv. Mater.* **2006**, *18* (1), 77–79.
- (7) McDonald, S. A.; Konstantatos, G.; Zhang, S. G.; Cyr, P. W.; Klem, E. J. D.; Levina, L.; Sargent, E. H. *Nat. Mater.* **2005**, *4* (2), 138–U14.
- (8) Maria, S.; Susha, A. S.; Sommer, M.; Talapin, D. V.; Rogach, A. L.; Thelakkat, M. *Macromolecules* **2008**, *41* (16), 6081–6088.
- (9) Alivisatos, A. P. *Science* **1996**, *271* (5251), 933–937.
- (10) Rogach, A. L. *Semiconductor nanocrystal quantum dots: synthesis, assembly, spectroscopy, and applications*; Springer: Wien; New York, 2008.
- (11) Leatherdale, C. A.; Kagan, C. R.; Morgan, N. Y.; Empedocles, S. A.; Kastner, M. A.; Bawendi, M. G. *Phys. Rev. B* **2000**, *62* (4), 2669–2680.
- (12) Coe, S.; Woo, W. K.; Bawendi, M.; Bulovic, V. *Nature* **2002**, *420* (6917), 800–803.
- (13) Kohary, K.; Burlakov, V. M.; Pettifor, D. G.; Burlakov, V. M.; Pettifor, D. G. *J. Appl. Phys.* **2006**, *100* (11), 114315.
- (14) Forrest, S. R. *Nature* **2004**, *428* (6986), 911–918.
- (15) Greenham, N. C.; Peng, X. G.; Alivisatos, A. P. *Phys. Rev. B* **1996**, *54* (24), 17628–17637.
- (16) Kaufmann, S.; Stoferle, T.; Moll, N.; Mahrt, R. F.; Scherf, U.; Tsami, A.; Talapin, D. V.; Murray, C. B. *Appl. Phys. Lett.* **2007**, *90* (7), 071108.
- (17) Chang, T. W. F.; Musikhin, S.; Bakueva, L.; Levina, L.; Hines, M. A.; Cyr, P. W.; Sargent, E. H. *Appl. Phys. Lett.* **2004**, *84* (21), 4295–4297.
- (18) Anni, M.; Manna, L.; Cingolani, R.; Valerini, D.; Creti, A.; Lomascoco, M. *Appl. Phys. Lett.* **2004**, *85* (18), 4169–4171.
- (19) Stoferle, T.; Scherf, U.; Mahrt, R. F. *Nano Lett.* **2009**, *9* (1), 453–456.
- (20) Huang, F.; Wu, H. B.; Wang, D.; Yang, W.; Cao, Y. *Chem. Mater.* **2004**, *16* (4), 708–716.
- (21) Valeur, B. *Molecular fluorescence: principles and applications*; Wiley-VCH: Weinheim, Germany, 2002.
- (22) Kapitonov, A. M.; Stupak, A. P.; Gaponenko, S. V.; Petrov, E. P.; Rogach, A. L.; Eychmuller, A. *J. Phys. Chem. B* **1999**, *103* (46), 10109–10113.
- (23) Schlegel, G.; Bohnenberger, J.; Potapova, I.; Mews, A. *Phys. Rev. Lett.* **2002**, *88* (13), 137401.
- (24) Al Salman, A.; Tortschanoff, A.; van der Zwan, G.; van Mourik, F.; Chergui, M. *Chem. Phys.* **2009**, *357*, 96–101.
- (25) Ebenstein, Y.; Mokari, T.; Banin, U. *Appl. Phys. Lett.* **2002**, *80* (21), 4033–4035.
- (26) Brabec, C. J.; Zerza, G.; Cerullo, G.; De Silvestri, S.; Luzzati, S.; Hummelen, J. C.; Sariciftci, S. *Chem. Phys. Lett.* **2001**, *340* (3–4), 232–236.
- (27) Dexter, D. L. *J. Chem. Phys.* **1953**, *21* (5), 836–850.
- (28) Grell, M.; Bradley, D. D. C.; Long, X.; Chamberlain, T.; Inbasekaran, M.; Woo, E. P.; Soliman, M. *Acta Polym.* **1998**, *49* (8), 439–444.
- (29) Fytas, G.; Nothofer, H. G.; Scherf, U.; Vlassopoulos, D.; Meier, G. *Macromolecules* **2002**, *35* (2), 481–488.
- (30) Rogach, A. L.; Franzl, T.; Klar, T. A.; Feldmann, J.; Gaponik, N.; Lesnyak, V.; Shavel, A.; Eychmuller, A.; Rakovich, Y. P.; Donegan, J. F. *J. Phys. Chem. C* **2007**, *111*, 14628–14637.
- (31) Neher, D. *Macromol. Rapid Commun.* **2001**, *22*, 1365–1385.

NL900978A